Journal of Physics: Conference Series

PAPER • **OPEN ACCESS**

Wave transmission from asymmetrical changes of cross-sectional area in a beam

To cite this article: B E Takiuti *et al* 2019 *J. Phys.: Conf. Ser.* **1264** 012056

IOP Conf. Series: Journal of Physics: Conf. Series **1264** (2019) 012056 doi:10.1088/1742-6596/1264/1/012056

Wave transmission from asymmetrical changes of cross-sectional area in a beam

B E Takiuti[1], E Manconi[2], M J Brennan[1], V Lopes Junior[1]

[1] Department of Mechanical Engineering, UNESP - São Paulo State University, Av. Brasil Sul, 56 - Centro, Ilha Solteira - SP, 15385-000 Brazil
E-mail: takiuti.breno@gmail.com
[2] Department of Industrial Engineering, University of Parma, Viale delle Scienze 181/A, 43100 Parma, Italy
E-mail: elisabetta.manconi@unipr.it

Abstract. In this paper wave scattering from an asymmetrical change of cross-sectional area in a beam is numerically studied. Incident symmetric and antisymmetric Lamb waves are considered and multiple wave mode conversion due to interaction with the discontinuity are investigated up to high frequency (above the cut-off of the second symmetric Lamb wave mode, S_2). Results are presented in terms of transmission power coefficients, kinetic energy, and energy velocity. These are evaluated using the Wave Finite Element method to predict the wave modes from FE cross-sectional nodal displacements and nodal forces. It is shown that the methodology proposed can give an insight into wave scattering and multiple converted Lamb wave modes, which can be useful in Structural Health Monitoring.

Keywords: finite element, wave scattering, damage detection, structural health monitoring

1. Introduction

Ultrasonic guided waves are used in Structural Health Monitoring (SHM) for damage detection [1]. The effectiveness of proper strategies for damage diagnosis and detection using this technique strongly rely on the prediction of wave propagation and wave scattering behaviour.

In this paper wave scattering in a beam with asymmetric variations of the cross-sectional area (notch) is numerically investigated. This situation can be representative of general defects, open cracks, or damage due to corrosion in one-dimensional waveguides. Several authors have investigated the problem at different frequency ranges and by different approaches/methodologies. Lamb wave interaction with notches in a plate was studied in [2] and at low frequency in [3, 4] using Finite Element Analysis. In [5] a hybrid Boundary Element Method was applied to investigate wave scattering caused by elliptical shape defects in plates, while symmetric and asymmetric step discontinuities in plates were studied in [6] using the same method and in [7] using an analytical approach. A numerical approach based on the Scaled Boundary Finite Element Method was also presented in [8], where wave interaction with defects in plates was predicted. Asymmetrical notches were studied in [9], where a technique to separate the fundamental wave mode contribution in the scattered waves at low frequency was proposed.

Amongst other methods, the Wave Finite Element (WFE) [10, 11] has been recently applied for the prediction of wave scattering in [12-16]. The method is applied in the present work to find the scattering matrix from a notch in beams assuming pure antisymmetric A_0 and symmetric S_0 fundamental Lamb

wave mode excitation. The scattering problem is formulated modelling the damaged beam in three parts: undamaged, damaged, undamaged. Each of these parts is considered as an infinite waveguide whose wave characteristics, wave modes and dispersion curves, are easily obtained using the WFE method. Nodal displacements and nodal forces are approximated using these wave modes as a basis. The undamaged and damaged parts are then coupled using continuity of displacement and force equilibrium as in [17]. The methodology, exploiting standard FE discretisation of a small segment of the waveguide, can be applied to one-dimensional waveguides with complex cross-sectional characteristic with the same degree of difficulty.

The paper is organised as follows. In the first section, the method is outlined, and the main steps to obtain the scattering matrix, power coefficients, kinetic energy and energy velocity are given. In section 2 numerical results are shown and the method is then used to determine power coefficients and transmitted kinetic energy from a notch in an isotropic beam assuming pure antisymmetric A_0 and symmetric S_0 Lamb wave mode excitation. Numerical results are shown for a wide frequency range - above the cut-off of the second symmetric Lamb wave mode (S_2). The effect of the depth variation of the notch is then investigated in terms of scattered kinetic energy and energy velocity. In particular, wave mode conversion is investigated evaluating the component in the horizontal and vertical direction of the kinetic energy and the energy velocity. The main results are finally summarised in Section 3.

2. Wave scattering from thickness variation using the WFE discretisation

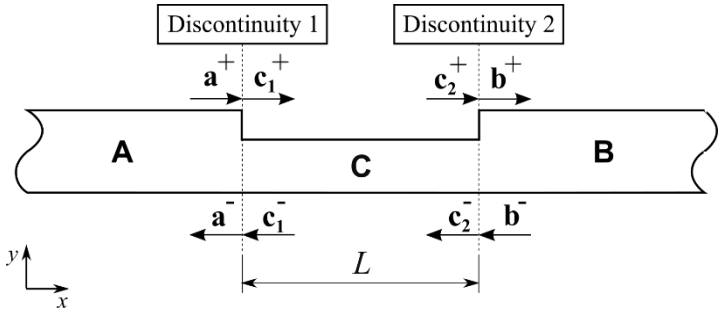

Figure 1. Schematic representation of a damaged waveguide with wave reflection and transmission at the discontinuities.

Figure 1 shows a schematic representation of the damaged waveguide, where x is propagation direction and the variation of the thickness is modelled as two subsequent step discontinuities between waveguides **A** and **C** and waveguides **C** and **B**. According to this, the right- and left-going incident waves at the discontinuities are grouped into vectors $[\mathbf{a}^+ \;\; \mathbf{c}_1^-]^T$ and $[\mathbf{c}_2^- \;\; \mathbf{b}^+]^T$, and the resulting left- and right-going scattered waves in $[\mathbf{a}^- \;\; \mathbf{c}_1^+]^T$ and $[\mathbf{c}_2^+ \;\; \mathbf{b}^-]^T$.

The wave amplitudes at the two discontinuities in waveguide **C** can be related by a transfer matrix $\mathbf{T}_\mathrm{C} = \mathrm{diag}\left[\exp\left(-\mathrm{i}\mathbf{k}_\mathrm{C} L\right)\right]$, that is

$$\mathbf{c}_2^+ = \mathbf{T}_\mathrm{C}\mathbf{c}_1^+, \quad \mathbf{c}_1^- = \mathbf{T}_\mathrm{C}^{-1}\mathbf{c}_2^- \tag{1}$$

For each waveguide, nodal displacements $\mathbf{\Phi}_\mathbf{q}$ (wave modes), nodal forces $\mathbf{\Phi}_\mathbf{f}$, and dispersion curves $(\mathbf{k},\omega)$ are obtained using the WFE method [10-12]. These are grouped into positive and negative going waves including all the evanescent and complex wave modes: for example $\left(\omega, \mathbf{k}_\mathrm{A}{}^+, \; \mathbf{\Phi}_\mathrm{A}{}^+ = [\mathbf{\Phi}_{\mathbf{q},\mathrm{A}}^+, \mathbf{\Phi}_{\mathbf{f},\mathrm{A}}^+]^T\right)$ and $\left(\omega, \mathbf{k}_\mathrm{A}{}^-, \mathbf{\Phi}_\mathrm{A}{}^- = [\mathbf{\Phi}_{\mathbf{q},\mathrm{A}}^-, \mathbf{\Phi}_{\mathbf{f},\mathrm{A}}^-]^T\right)$ for waveguide **A** and using a similar notation for waveguides **C** and **B**.

The discontinuities in Fig. 1(a) are described using a state vector consisting of a vector of nodal displacements **q** and nodal internal forces **f**. These can be described in the wave domain as

$$\begin{Bmatrix}\mathbf{q}_{\mathsf{A}}\\ \mathbf{f}_{\mathsf{A}}\end{Bmatrix}=\begin{bmatrix}\boldsymbol{\Phi}^{+}_{\mathbf{q},\mathsf{A}} & \boldsymbol{\Phi}^{-}_{\mathbf{q},\mathsf{A}}\\ \boldsymbol{\Phi}^{+}_{\mathbf{f},\mathsf{A}} & \boldsymbol{\Phi}^{-}_{\mathbf{f},\mathsf{A}}\end{bmatrix}\begin{Bmatrix}\mathbf{a}^{+}\\ \mathbf{a}^{-}\end{Bmatrix},\ \begin{Bmatrix}\mathbf{q}_{\mathsf{B}}\\ \mathbf{f}_{\mathsf{B}}\end{Bmatrix}=\begin{bmatrix}\boldsymbol{\Phi}^{+}_{\mathbf{q},\mathsf{B}} & \boldsymbol{\Phi}^{-}_{\mathbf{q},\mathsf{B}}\\ \boldsymbol{\Phi}^{+}_{\mathbf{f},\mathsf{B}} & \boldsymbol{\Phi}^{-}_{\mathbf{f},\mathsf{B}}\end{bmatrix}\begin{Bmatrix}\mathbf{b}^{+}\\ \mathbf{b}^{-}\end{Bmatrix},\ \begin{Bmatrix}\mathbf{q}_{\mathsf{C}_{1,2}}\\ \mathbf{f}_{\mathsf{C}_{1,2}}\end{Bmatrix}=\begin{bmatrix}\boldsymbol{\Phi}^{+}_{\mathbf{q},\mathsf{C}} & \boldsymbol{\Phi}^{-}_{\mathbf{q},\mathsf{C}}\\ \boldsymbol{\Phi}^{+}_{\mathbf{f},\mathsf{C}} & \boldsymbol{\Phi}^{-}_{\mathbf{f},\mathsf{C}}\end{bmatrix}\begin{Bmatrix}\mathbf{c}_{1,2}{}^{+}\\ \mathbf{c}_{1,2}{}^{-}\end{Bmatrix} \quad (2)$$

where the subscripts **f** and **q** correspond to the wave mode matrices $\boldsymbol{\Phi}^{\pm}_{\mathbf{f}}$ and $\boldsymbol{\Phi}^{\pm}_{\mathbf{q}}$, and the subscripts **A** and **B** and **C** indicate the waveguide. A reduced wave basis can be used to describe displacements and internal forces. However, the choice of the modes to describe the displacement and give a correct representation of the scattering is not a trivial task. The number of waves retained can be different at different frequencies and is related to the model size. All propagating waves (pure real wavenumbers) must be retained. Evanescent (pure imaginary wavenumber) and attenuating waves (complex wavenumbers) contribute to the energy redistribution amongst modes and they must be included since they give fundamental contributions in most of the scattering problems. Since the discontinuities are conservative, all the propagating modes are considered while the number of evanescent and complex modes is estimated by the convergence of the sum of the absolute value of the reflected and transmitted power coefficients, see Eq. (8), to $1+\varepsilon$, where ε is a small error. This corresponds to choosing the number of modes that gives the minimum difference between the sum of the total reflected and transmitted energy flow, and the incident energy flow.

In order to obtain the scattering matrix, the continuity of displacement and equilibrium of nodal forces at 1 and 2 can be written using a general matrix formulation as

$$\begin{aligned}&\mathbf{Q}_{\mathsf{A}}\mathbf{q}_{\mathsf{A}}=\mathbf{Q}_{\mathsf{C}_1}\mathbf{q}_{\mathsf{C}_1},\quad \mathbf{F}_{\mathsf{A}}\mathbf{f}_{\mathsf{A}}=\mathbf{F}_{\mathsf{C}_1}\mathbf{f}_{\mathsf{C}_1}\\ &\mathbf{Q}_{\mathsf{C}_2}\mathbf{q}_{\mathsf{C}_2}=\mathbf{Q}_{\mathsf{B}}\mathbf{q}_{\mathsf{B}},\quad \mathbf{F}_{\mathsf{C}_2}\mathbf{f}_{\mathsf{C}_2}=\mathbf{F}_{\mathsf{B}}\mathbf{f}_{\mathsf{B}}\end{aligned} \quad (3)$$

The use of Eqs. (2) and (3), enables the wave amplitudes at the discontinuities to be obtained as

$$\begin{Bmatrix}\mathbf{a}^{-}\\ \mathbf{c}_1^{+}\end{Bmatrix}=\begin{bmatrix}\mathbf{R}_1^{\mathsf{AA}} & \mathbf{T}_1^{\mathsf{AC}}\\ \mathbf{T}_1^{\mathsf{CA}} & \mathbf{R}_1^{\mathsf{CC}}\end{bmatrix}\begin{Bmatrix}\mathbf{a}^{+}\\ \mathbf{c}_1^{-}\end{Bmatrix},\quad \begin{Bmatrix}\mathbf{c}_2^{-}\\ \mathbf{b}^{+}\end{Bmatrix}=\begin{bmatrix}\mathbf{R}_2^{\mathsf{CC}} & \mathbf{T}_2^{\mathsf{CB}}\\ \mathbf{T}_2^{\mathsf{BC}} & \mathbf{R}_2^{\mathsf{BB}}\end{bmatrix}\begin{Bmatrix}\mathbf{c}_2^{+}\\ \mathbf{b}^{-}\end{Bmatrix} \quad (4)$$

Eq. (1) and Eqs. (4) are then further combined in order to give the total scattering matrix for the waveguide, that is

$$\begin{Bmatrix}\mathbf{a}^{-}\\ \mathbf{b}^{+}\end{Bmatrix}=\begin{bmatrix}\mathbf{R}^{\mathsf{AA}} & \mathbf{T}^{\mathsf{AB}}\\ \mathbf{T}^{\mathsf{BA}} & \mathbf{R}^{\mathsf{BB}}\end{bmatrix}\begin{Bmatrix}\mathbf{a}^{+}\\ \mathbf{b}^{-}\end{Bmatrix} \quad (5)$$

Without loss of generality, it can be assumed that incident waves are coming from waveguide **A**, that is $\mathbf{a}^{+}$ is assumed to be given and known while $\mathbf{b}^{-}=0$. In this case, combining Eq. (1) and Eqs. (4), the vector of reflected waves $\mathbf{a}^{-}$ and the vector of transmitted waves $\mathbf{b}^{+}$ are given by

$$\begin{aligned}&\mathbf{a}^{-}=\mathbf{R}^{\mathsf{AA}}\mathbf{a}^{+};\quad \mathbf{R}^{\mathsf{AA}}=\mathbf{R}_1^{\mathsf{AA}}+\mathbf{T}_1^{\mathsf{AC}}\mathbf{T}_{\mathsf{C}}\left(\mathbf{I}-\mathbf{T}_{\mathsf{C}}^{-1}\mathbf{R}_2^{\mathsf{CC}}\mathbf{T}_{\mathsf{C}}\mathbf{R}_1^{\mathsf{CC}}\right)^{-1}\mathbf{R}_2^{\mathsf{CC}}\mathbf{T}_{\mathsf{C}}\mathbf{T}_1^{\mathsf{CA}}\\ &\mathbf{b}^{+}=\mathbf{T}^{\mathsf{BA}}\mathbf{a}^{+};\quad \mathbf{T}^{\mathsf{BA}}=\mathbf{T}_2^{\mathsf{BC}}\mathbf{T}_{\mathsf{C}}^{-1}\left(\mathbf{I}-\mathbf{T}_{\mathsf{C}}\mathbf{R}_1^{\mathsf{CC}}\mathbf{T}_{\mathsf{C}}^{-1}\mathbf{R}_2^{\mathsf{CC}}\right)^{-1}\mathbf{T}_1^{\mathsf{CA}}\end{aligned} \quad (6)$$

where **I** is the identity matrix.

From Eq. (1), the displacement and forces associated with the incident, reflected and transmitted waves are therefore evaluated as

$$\begin{aligned}\mathbf{q}_{\mathrm{I}} &= \mathbf{\Phi}^{+}_{\mathbf{q},\mathrm{A}}\mathbf{a}^{+};\quad \mathbf{q}_{\mathrm{R}} = \mathbf{\Phi}^{-}_{\mathbf{q},\mathrm{A}}\mathbf{R}^{\mathrm{AA}}\mathbf{a}^{+};\quad \mathbf{q}_{\mathrm{T}} = \mathbf{\Phi}^{+}_{\mathbf{q},\mathrm{B}}\mathbf{T}^{\mathrm{BA}}\mathbf{a}^{+}\\ \mathbf{f}_{\mathrm{I}} &= \mathbf{\Phi}^{+}_{\mathbf{f},\mathrm{A}}\mathbf{a}^{+};\quad \mathbf{f}_{\mathrm{R}} = \mathbf{\Phi}^{-}_{\mathbf{f},\mathrm{A}}\mathbf{R}^{\mathrm{AA}}\mathbf{a}^{+};\quad \mathbf{f}_{\mathrm{T}} = \mathbf{\Phi}^{+}_{\mathbf{f},\mathrm{B}}\mathbf{T}^{\mathrm{BA}}\mathbf{a}^{+}\end{aligned} \tag{7}$$

where subscripts *I, R, T*, refer to the incident, reflected and transmitted waves. From Eq. (7), the incident reflected and transmitted time-averaged energy flows can be evaluated by $\Pi_{\mathrm{I}} = \frac{\omega}{2}\mathrm{Im}\left\{\mathbf{f}_{\mathrm{I}}^{H}\mathbf{q}_{\mathrm{I}}\right\}$, $\Pi_{\mathrm{R}} = \frac{\omega}{2}\mathrm{Im}\left\{\mathbf{f}_{\mathrm{R}}^{H}\mathbf{q}_{\mathrm{R}}\right\}$ and $\Pi_{\mathrm{T}} = \frac{\omega}{2}\mathrm{Im}\left\{\mathbf{f}_{\mathrm{T}}^{H}\mathbf{q}_{\mathrm{T}}\right\}$ [10], where *H* denotes Hermitian transpose, while the reflection and transmission power coefficients are given by ratios

$$\nu = \frac{\Pi_{\mathrm{R}}}{\Pi_{\mathrm{I}}} = \frac{\mathrm{Im}\left\{\mathbf{f}_{\mathrm{R}}^{H}\mathbf{q}_{\mathrm{R}}\right\}}{\mathrm{Im}\left\{\mathbf{f}_{\mathrm{I}}^{H}\mathbf{q}_{\mathrm{I}}\right\}},\quad \tau = \frac{\Pi_{\mathrm{T}}}{\Pi_{\mathrm{I}}} = \frac{\mathrm{Im}\left\{\mathbf{f}_{\mathrm{T}}^{H}\mathbf{q}_{\mathrm{T}}\right\}}{\mathrm{Im}\left\{\mathbf{f}_{\mathrm{I}}^{H}\mathbf{q}_{\mathrm{I}}\right\}} \tag{8}$$

One of the important aspects of Lamb wave scattering problems is the evaluation of the contribution of single wave modes when multimode scattering is involved. This is particularly important when mode conversion occurs due to asymmetric discontinuities since it leads to a better investigation of the scattering and the possibility of sizing the defect. When multi-wave modes are scattered, and in particular at high frequency when energy is redistributed amongst several higher order modes, prediction of the change in the time of flight of the reflected and transmitted wave field, together with the level of mode conversion, can be assessed evaluating the reflected and transmitted energy velocities and the directional components of the time-averaged kinetic energy. The latter can also give important information about the frequency range in which the scattered displacement signal has a maximum amplitude.

The time-averaged kinetic energies for the incident, reflected and transmitted wave fields are given by

$$\begin{aligned}\Gamma_{\mathrm{I}} &= \frac{(i\omega)^2}{4}\mathrm{Re}\left[\left(\mathbf{\Phi}^{+}_{\mathbf{q},\mathrm{A}}\mathbf{a}^{+}\right)^{H}\mathbf{M}_{\mathrm{A}}\left(\mathbf{\Phi}^{+}_{\mathbf{q},\mathrm{A}}\mathbf{a}^{+}\right)\right];\\ \Gamma_{\mathrm{R}} &= \frac{(i\omega)^2}{4}\mathrm{Re}\left[\left(\mathbf{\Phi}^{-}_{\mathbf{q},\mathrm{A}}\mathbf{R}^{\mathrm{AA}}\mathbf{a}^{+}\right)^{H}\mathbf{M}_{\mathrm{A}}\left(\mathbf{\Phi}^{-}_{\mathbf{q},\mathrm{A}}\mathbf{R}^{\mathrm{AA}}\mathbf{a}^{+}\right)\right];\\ \Gamma_{\mathrm{T}} &= \frac{(i\omega)^2}{4}\mathrm{Re}\left[\left(\mathbf{\Phi}^{+}_{\mathbf{q},\mathrm{B}}\mathbf{T}^{\mathrm{BA}}\mathbf{a}^{+}\right)^{H}\mathbf{M}_{\mathrm{B}}\left(\mathbf{\Phi}^{+}_{\mathbf{q},\mathrm{B}}\mathbf{T}^{\mathrm{BA}}\mathbf{a}^{+}\right)\right]\end{aligned} \tag{9}$$

The expressions in Eq. (9) are here evaluated assuming a sufficient distance from the discontinuity in order to satisfy a far-field scattering condition. Therefore, only propagating modes with real wavenumber are taken into account in Eq. (9) (it should be noted that the scattering matrix must be evaluated considering the contribution of propagating, complex and nearfield as described previously).

The energy velocity is calculated as the ratio between the time-averaged energy flow and the time average total energy density per unit length, [10]. For example, the expression of the energy velocity of the incident wave field is

$$c_{e\mathrm{I}} = \frac{\frac{\omega}{2}\mathrm{Im}\left\{\mathbf{f}_{\mathrm{I}}^{H}\mathbf{q}_{\mathrm{I}}\right\}}{\frac{(i\omega)^2}{4\Delta}\mathrm{Re}\left[\left(\mathbf{\Phi}^{+}_{\mathbf{q},\mathrm{A}}\mathbf{a}^{+}\right)^{H}\mathbf{M}_{\mathrm{A}}\left(\mathbf{\Phi}^{+}_{\mathbf{q},\mathrm{A}}\mathbf{a}^{+}\right)\right]+\frac{1}{4\Delta}\mathrm{Re}\left[\left(\mathbf{\Phi}^{+}_{\mathbf{q},\mathrm{A}}\mathbf{a}^{+}\right)^{H}\mathbf{K}_{\mathrm{A}}\left(\mathbf{\Phi}^{+}_{\mathbf{q},\mathrm{A}}\mathbf{a}^{+}\right)\right]} \tag{10}$$

with similar expressions for the reflected and transmitted energy velocities. For dispersive uniform lossless waveguides, this equals the group velocity, which is cinematically defined as $c_g = \mathrm{d}\omega/\mathrm{d}k$. However, when damped structures and spatially attenuated wave modes are of concern, the group velocity can yield non-physical solutions. Therefore, the energy velocity seems to be more appropriate to quantify the velocity of energy transport.

3. Numerical results

An isotropic steel waveguide with an asymmetric notch of length L is considered. Figure 2 shows a schematic model of the WFE discretisation of the damaged waveguide, where a small segment of length Δ for each waveguide is discretised using FE plane elements in plane strain.

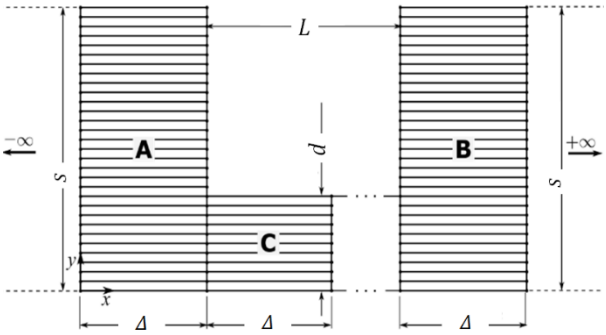

Figure 2. Schematic representation of the WFE discretisation of the damaged waveguide.

An investigation into the scattered waves has shown that, even when a pure mode is excited, a number of other modes are generated by the interaction of the excited wave with the asymmetric defects according to the waveguide characteristics and the frequency range of interest. Moreover, evanescent and complex modes cannot be neglected since they account for energy distribution of the scattering. Attention must be paid to the number of modes included in the analysis. Therefore, the prediction of the complex dispersion curves of the structure including higher order modes is essential in the investigation of reflected and transmitted wave characteristics.

Figure 3 shows the complex dispersion curves of the waveguide obtained applying the WFE method when the depth of the notch is assumed to be 40% of the waveguide thickness. The non-dimensional parameters $\mu = k\Delta$ and $\Omega = \omega/\omega_{\text{cut-off}}$ are introduced, where k is the wavenumber, $\Delta = 6\cdot10^{-5}$ m is the length of the WFE segment in the x-direction, and $\omega_{\text{cut-off}}$ is the cut-off frequency of the first antisymmetric Lamb mode (A_1) of the thicker waveguide. The length of the damage is assumed to be $L = 33.4\cdot10^{3}\Delta$ while the percentage of damage refers to the ratio $(s-d)/d$, where s is the thickness of the waveguide (waveguide **A** and **B**) and d is the thickness of the damaged waveguide (waveguide **C**) as in Fig. 2. It can be seen that cut-off frequencies occur at $\Omega = 1;\ 1.75;\ 1.89$ and 2.02 for waveguide **A** and **B,** and at $\Omega = 1.68$ for waveguide **C**. It is also clear from Fig. 3 that the number of wave modes to be considered in the wave mode expansion in Eq. (2), must change according to the frequency range under analysis.

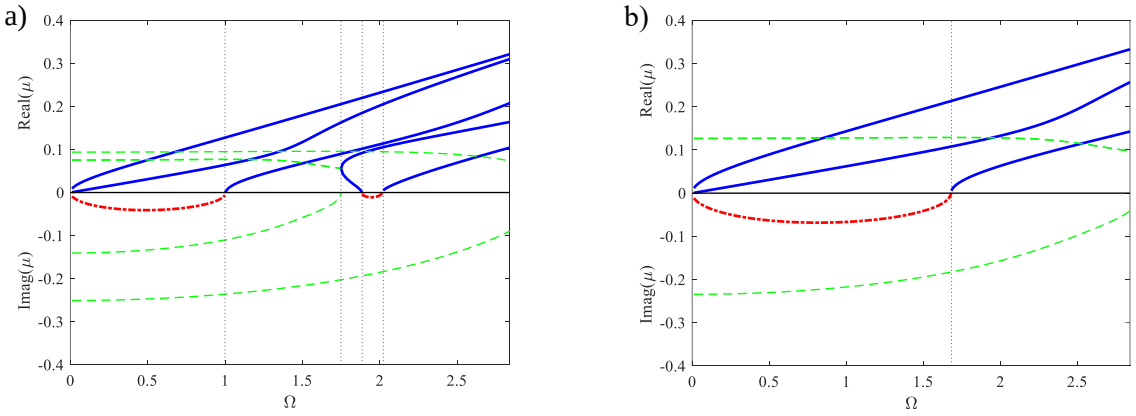

Figure 3. Dispersion curves, 40% of damage: a) waveguide **A** and **B**; b) waveguide **C**. ——— propagating modes; – · – · – : evanescent modes; – – – : complex modes (note that complex modes occur as a pair of complex conjugate modes, and only one of the pairs with positive real and negative imaginary parts are shown here). The vertical lines correspond to cut-off frequencies.

Figs. 4 and 5 show the scattering behaviour, assuming that the first symmetric S_0 and antisymmetric A_0 Lamb wave modes are selectively excited to propagate in waveguide **A**. The figures show the power coefficients and time-averaged kinetic energy component in the horizontal and vertical directions, i.e., the *x* and *y*-directions for the models in Figs. 1 and 2. The time-averaged kinetic energy was evaluated assuming a sufficient distance from the discontinuity in order to satisfy a far-field scattering condition, that is only propagating modes with real wavenumber are considered – it should be noted that the scattering matrix must be evaluated considering the contribution of propagating, complex and nearfield waves as described in the previous section.

Fig 4(a) and 5(a) show the time-averaged energy flow of the scattered waves. At low frequency, the power coefficients show similar behaviour and most of the energy is transmitted in both cases below the first cut-off frequency. The behaviour of the power coefficients become more complicated at higher frequencies with maxima and minima at the higher cut-off frequencies, where new propagating modes with in-plane and out-of-plane displacements start propagating. In particular, a change in behaviour occurs at the first cut-off due to the energy redistribution through the A_1 wave mode in the thicker waveguide. Above this frequency, the behaviour changes significantly for the case of the A_0 incident wave mode at the first cut-off frequency for waveguide **C**, $\Omega = 1.68$ as shown in Fig. 4(a). The nearfield transverse mode in waveguide **C** starts to propagate, and there is a significant increase in the reflected power with a commensurate decrease in the transmitted power. At $\Omega = 1.68$ all the energy is reflected, which then decreases to a local minimum at $\Omega = 2.02$ due to the cut-off frequency of a new higher mode in the thicker waveguide. Above the fourth cut-off frequency, about 60% of the energy is transmitted and 40% is reflected. This does not happen in Fig 5(a) due to the different nature of the incident wave mode, although local maxima and minima follow the same trend at the cut-off frequencies.

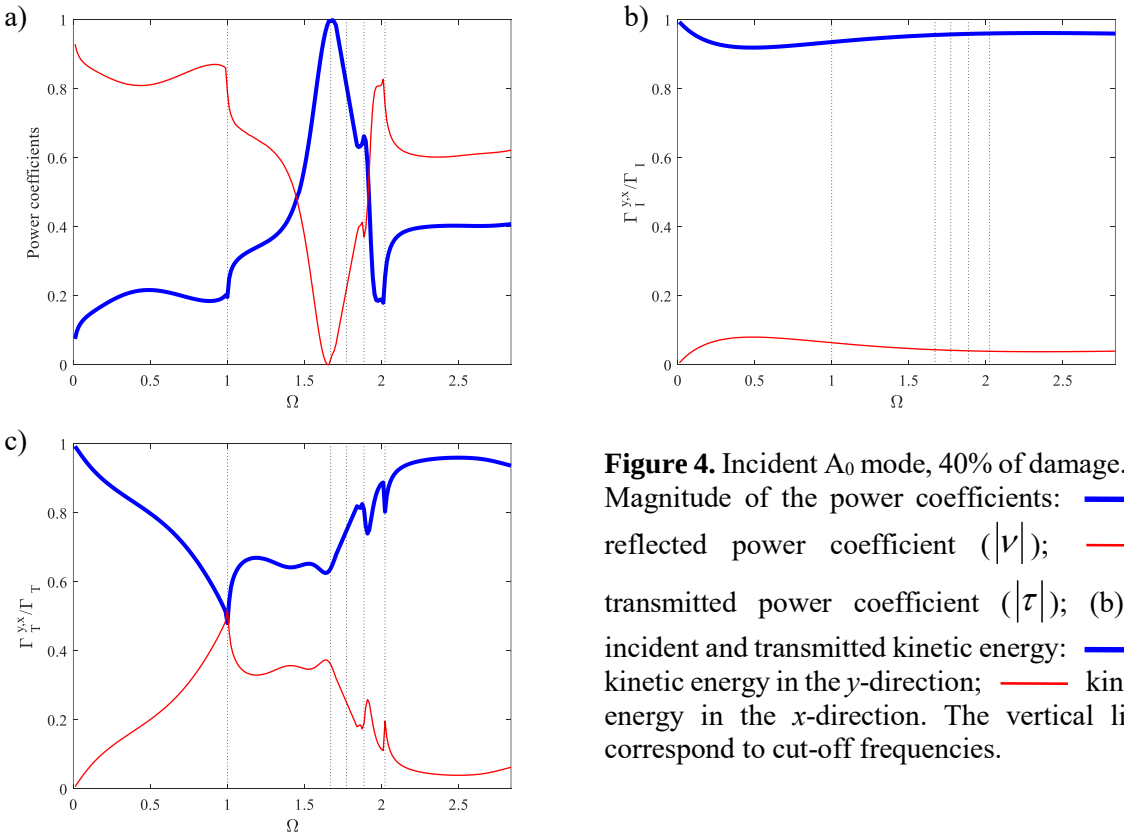

Figure 4. Incident A_0 mode, 40% of damage. (a) Magnitude of the power coefficients: reflected power coefficient ($|\nu|$); transmitted power coefficient ($|\tau|$); (b)-(c) incident and transmitted kinetic energy: kinetic energy in the *y*-direction; kinetic energy in the *x*-direction. The vertical lines correspond to cut-off frequencies.

Figs. 4(b) and 5(b) show the time-averaged kinetic energy of the incident wave in the *x* and *y*-directions compared to the total incident kinetic energy, showing the nature of the cross-sectional displacement under the passage of the wave. In can be seen that for the A_0 incident wave mode, greater than 90% of the energy is in the *y*-direction and the mode maintains its main transverse characteristics for all frequencies. This is not the case for the incident S_0 mode. The energy in the *x*-direction is above 90% at low frequency, then it gradually decreases to less than 10% with a corresponding gradually increase of the energy in the *y*-direction up to 90%. The two components show the same value at $\Omega = 1.423$. This change in the behaviour of mode S_0 can be identified by examining the dispersion curves in Fig. 3.

Evaluation of the components of the transmitted kinetic energy can give an insight into the level asymmetry of the damage. In the case of a symmetric damage, the components of the kinetic energy of the incident and scattered waves are similar in nature, since mode conversion occurs only between wave modes with the same characteristics, which does not hold for the asymmetric defect.

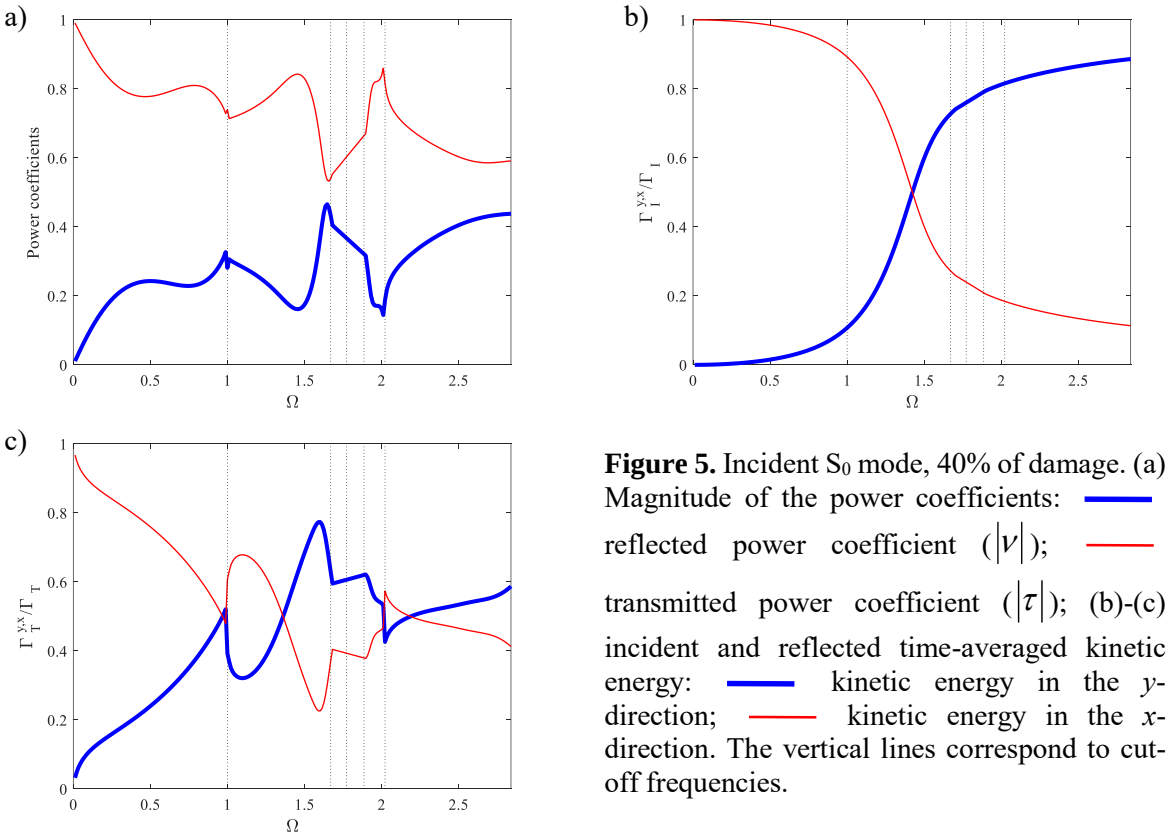

Figure 5. Incident S_0 mode, 40% of damage. (a) Magnitude of the power coefficients: reflected power coefficient ($|\nu|$); transmitted power coefficient ($|\tau|$); (b)-(c) incident and reflected time-averaged kinetic energy: kinetic energy in the *y*-direction; kinetic energy in the *x*-direction. The vertical lines correspond to cut-off frequencies.

Figs. 4(c) and 5(c) show that, for both A_0 and S_0 incident waves, the effect of the asymmetric defect in terms of mode conversion is particularly significant in the transmitted kinetic energy above the first cut-off frequency. However, in general, the behaviour in both cases becomes more complicated above the first cut-off frequency, where higher order modes are reflected and transmitted, and mode conversion of the incident wave field becomes significant. Below the first cut-off frequency, the main directional components of the kinetic energy associated to the incident mode, which are the *y* component for the incident A_0 wave and the *x* component for the incident S_0 wave, decrease almost monotonically to reach the same value, so that at $\Omega = 1$ the kinetic energy is equally distributed in the *x* and *y*-directions. Above this frequency the behaviour changes. In the case of the asymmetric incident wave, which is illustrated in Fig. 4(c), the component in the *y*-direction increases, and above the fourth cut-off more than 90% of the energy is transmitted in the *y*-direction. For the S_0 incident wave, above $\Omega = 1$ the component in the *x*-direction increases up to a local maximum, then decreases to a minimum at $\Omega = 1.68$, which corresponds to the cut-off of the A_1 wave mode in waveguide **C**. It can be seen that at $\Omega = 1.423$ the two components have the same value which is the same as the incident mode as can be seen in Fig. 5(b). Above the fourth cut-off frequency, the displacement in the *y*-direction is greater than that in the *x*-direction.

The effects of the variation of the thickness of the damage on the transmitted waves are shown in Fig. 6. Although the A_0 wave mode is dispersive at low frequency, it becomes less dispersive at higher frequencies compared to the S_0 wave mode. Moreover, its characteristics remain similar throughout the whole frequency range. More than 90% of the amplitude of the cross-sectional displacement of the incident mode is in the *y*-direction, which is not the case for the S_0 mode as shown previously. Therefore, the A_0 mode is preferred as the selectively excited wave to propagate as an incident mode. In all the cases the incident wavelength is comparable with the size of the notch

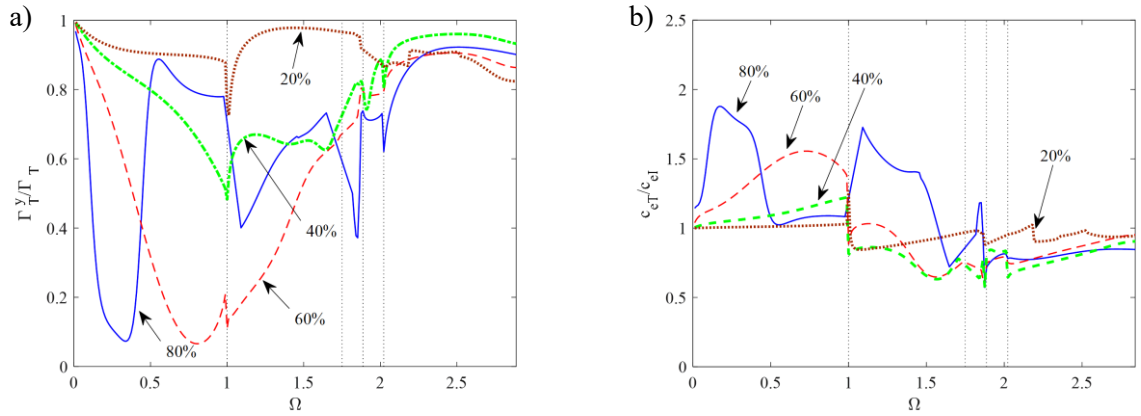

Figure 6. A_0 incident mode. a) Transmitted kinetic energy component in the *y*-directions for different depth of the damage; b) transmitted energy velocity over the incident energy velocity for different depth of the damage. The vertical lines correspond to cut-off frequencies in the thicker waveguide **A**.

Fig. 6(a) shows the transmitted kinetic energy components in the *y*-direction with respect to the overall level. It can be seen that in the case of 20% of notch depth, the behaviour of the transmitted kinetic energy has similar characteristics to the incident one shown in Fig. 4(b), apart from a minimum at the first cut-off frequency. Therefore, most of the energy is transmitted with the displacement in the *y*-direction. The *y* component of the transmitted displacement decreases with increasing of the damage size and has a lower minimum at the first cut-off frequency for a depth of the damage equal to 40%. Above this level, the differences become more significant due to the mode conversion caused by increasing loss of symmetry with respect to the neutral axis of the structure. In particular, when the damage reaches 60% and 80% with respect to the beam thickness, the minima occur below the first cut-off frequency with an abrupt decrease to almost a zero of the component in the *y*-direction. At these minima, the *x* component of the transmitted displacement is comparable with that of an S_0 mode even if a pure A_0 wave mode is incident. Above the fourth cut-off frequency, the *y* component of the transmitted wave increases up to a plateau at high frequency, with more than 80% of the cross-sectional displacement in the *y*-direction. This is independent of the thickness variation of the beam. As expected, the case of 80% of damage shows a more complicated behaviour with local maxima and minima due to significant mode conversion.

Fig. 6(b) shows the transmitted energy velocity $c_{e\mathrm{T}}$ with respect to the incident energy velocity $c_{e\mathrm{I}}$. In the figure, values close to unity have a velocity of the transmitted waves similar to that of the incident wave, showing no significant mode conversion. On the other hand, values significantly different from unity exhibit mode conversion and energy redistribution amongst different modes. The behaviour confirms the trend depicted in Fig. 6(a). Significant changes in the transmitted energy velocity with respect to that of the incident wave occur at the first cut-off frequency. These changes increase according to the loss of symmetry of the damaged part with respect to the neutral axis of the original waveguide. In particular, for a percentage of damage equal to 60% and 80%, a maximum occurs below the cut-off frequency for the thicker waveguide due to the greater energy velocity of the S_0 mode, which becomes predominant, compared to that of the incident mode. Again, at higher frequencies, most the energy is transmitted with a velocity close to the incident energy velocity.

4. Conclusions

In this work, a Wave Finite Element method has been applied to an investigation of Lamb wave transmission from a notch in beams up to high frequency. Although the method described, which exploits standard FE discretisation of the waveguide through the cross-section, can be easily applied to more complicated waveguides, numerical results have been given for an isotropic case to show some mode conversion characteristics.

It has been shown that even when a pure wave mode is excited, a number of other modes are generated by the interaction of the excited wave with the asymmetric defect. This phenomenon is known as mode conversion and it was investigated by the transmitted time-averaged kinetic energy in terms of its component in the vertical and horizontal direction. These, together with the energy velocity, have given insight into the complicated mode scattering when multi-modes are involved. Numerical results have been shown up to high frequency for different notch depths. It was seen that wave mode conversion depends not only upon the size of the damage (depth of the notch) and the level of asymmetry with respect to the neutral axis of the waveguide, but also on the thickness of the waveguide and the damaged part. This is due to the cut-off frequencies of symmetric and asymmetric modes according to the frequency range of interest.

When the incident wavelength is comparable with the size of the notch, reflection and transmission typically showed similar behaviour below the first cut-off frequency. However, at this frequency, the scattering behaviour changed drastically due to the cut-off frequency of the A_1 Lamb wave mode. Above the first cut-off frequency, there are also changes in the S_0 wave mode which is affected in terms of the directional component of the transmitted displacement and the energy velocity. Close to the cut-off frequencies of higher order modes, reflection and transmission become more complicated due to complex energy redistribution between the wave modes.

Acknowledgements
This study was financed in part by the Coordenação de Aperfeiçoamento de Pessoal de Nível Superior – Brasil (CAPES) – Finance Code 001 and it was partially carried out while the first author held a fellowship at the University of Parma, Italy, funded by the Ministero degli Affari Esteri Italiano. The authors gratefully acknowledge the financial support provided.

References

[1] Su Z, Ye L and Lu Y 2006 Guided Lamb waves for identification of damage in composite structures: A review *Journal of Sound and Vibration* **295** 753-80
[2] Alleyne D N and Cawley P 1992 The interaction of Lamb waves with defects *Ultrasonics, Ferroelectrics and Frequency Control, IEEE Transactions on* **39** 381-97
[3] Lowe M J S and Diligent O 2002 Low-frequency reflection characteristics of the s0 Lamb wave from a rectangular notch in a plate *The Journal of the Acoustical Society of America* **111** 64-74
[4] Lowe M J S, Cawley P, Kao J-Y and Diligent O 2002 The low frequency reflection characteristics of the fundamental antisymmetric Lamb wave a0 from a rectangular notch in a plate *The Journal of the Acoustical Society of America* **112** 2612-22
[5] Zhao X G and Rose J L 2003 Boundary element modeling for defect characterization potential in a wave guide *International Journal of Solids and Structures* **40** 2645-58
[6] Cho Y 2000 Estimation of ultrasonic guided wave mode conversion in a plate with thickness variation *IEEE Trans Ultrason Ferroelectr Freq Control* **47** 591-603
[7] Schaal C and Mal A 2016 Lamb wave propagation in a plate with step discontinuities *Wave Motion* **66** 177-89
[8] Gravenkamp H, Birk C and Song C 2015 Simulation of elastic guided waves interacting with defects in arbitrarily long structures using the Scaled Boundary Finite Element Method *Journal of Computational Physics* **295** 438-55
[9] Benmeddour F, Grondel S, Assaad J and Moulin E 2008 Study of the fundamental Lamb modes interaction with asymmetrical discontinuities *NDT & E International* **41** 330-40
[10] Mace B R, Duhamel D, Brennan M J and Hinke L 2005 Finite element prediction of wave motion in structural waveguides *The Journal of the Acoustical Society of America* **117** 2835-43
[11] Mace B R and Manconi E 2008 Modelling wave propagation in two-dimensional structures using finite element analysis *Journal of Sound and Vibration* **318** 884-902
[12] Renno J M, Manconi E and Mace B R 2013 A Finite Element Method for Modelling Waves in Laminated Structures *Advances in Structural Engineering* **16** 61-75

[13] Renno J M and Mace B R 2013 Calculation of reflection and transmission coefficients of joints using a hybrid finite element/wave and finite element approach *Journal of Sound and Vibration* **332** 2149-64
[14] Mitrou G, Ferguson N and Renno J 2017 Wave transmission through two-dimensional structures by the hybrid FE/WFE approach *Journal of Sound and Vibration* **389** 484-501
[15] Masri E, Ferguson N and Waters T 2017 Detecting damaged reinforcement bars in concrete structures using guided waves *Procedia Engineering* **199** 1882-7
[16] Apalowo R K, Chronopoulos D and Tanner G 2018 Wave Interaction with Defects in Pressurised Composite Structures *Journal of Nondestructive Evaluation* **37** 48
[17] Harland N R, Mace B R and Jones R W 2001 Wave propagation, reflection and transmission in tunable fluid-filled beams *Journal of Sound and Vibration* **241** 735-54